Clinical Science (2020) **134** 439–458
https://doi.org/10.1042/CS20191028

PORTLAND PRESS

Research Article

Myriocin and D-PDMP ameliorate atherosclerosis in ApoE$^{-/-}$ mice via reducing lipid uptake and vascular inflammation

Zemou Yu[1,*], Qing Peng[1,*], Songyue Li[2], Hongjun Hao[1], Jianwen Deng[1], Lingbing Meng[3], Zhiyuan Shen[1], Weiwei Yu[1], Ding Nan[1], Yu Bai[2] and Yining Huang[1]

[1]Department of Neurology, Peking University First Hospital, No. 8 Xishiku Street, Xicheng District, Beijing 100034, China; [2]Beijing National Laboratory for Molecular Sciences, Key Laboratory of Bioorganic Chemistry and Molecular Engineering of Ministry of Education, Institute of Analytical Chemistry, College of Chemistry and Molecular Engineering, Peking University, Beijing 100871, China; [3]Department of Neurology, Beijing Hospital, National Center of Gerontology, No.1 Dahua Road, Dong Dan, Beijing 100730, China

Correspondence: Yining Huang (ynhuang@bjmu.edu.cn) or Yu Bai (yu.bai@pku.edu.cn)

Sphingolipids have been implicated in the etiology of atherosclerosis. The commonly used sphingolipid inhibitors, myriocin (a ceramide inhibitor) and D-PDMP (D-threo-1-phenyl-2-decanoylamino-3-morpholino-1-propanol, a glycosphingolipid inhibitor), have shown therapeutic potential but their efficacy and their underlying mechanisms remain unclear. Here, apolipoprotein E-deficient (apoE$^{-/-}$) mice were fed a high-fat diet (HFD) and treated with a control, myriocin, D-PDMP, or atorvastatin for 12 weeks. We analyzed the effects of these drugs on the size and detailed composition of atherosclerotic plaques. Molecular biological approaches were used to explore how the inhibitors affect lipid metabolism and foam-cell formation. Treatment with myriocin or D-PDMP led to smaller and less vulnerable atherosclerotic lesions and was almost as effective as atorvastatin. Sphingolipid inhibitors down-regulated the expression of monocyte chemotactic protein 1 (MCP-1) and its receptor chemoattractant cytokine receptor 2 (CCR2), which play a key role in monocyte recruitment. They also decreased pro-inflammatory Ly-6c^{high} monocytes and influenced the uptake of modified LDL by down-regulating the expression of cluster of differentiation 36 (CD36) and lectin-like oxidized LDL (ox-LDL) receptor-1 (LOX-1). The inhibitors exhibited the advantage of maintaining normal glucose homeostasis compared with atorvastatin. These findings reveal for the first time that the modulation of sphingolipid synthesis can effectively alleviate atherosclerosis progression by preventing lipid uptake and reducing inflammatory responses in the arterial walls.

Introduction

Atherosclerosis is the fundamental pathological process underlying cardio-cerebral vascular diseases (CVDs), which are the leading cause of morbidity and mortality worldwide. Dyslipidemia is a major contributor to the pathogenesis of plaque formation in these diseases. Much effort has been directed to developing agents that reduce serum low-density lipoprotein cholesterol (LDL-C), and the most effective drugs developed so far being statins [1]. It has been recognized that a significant number of patients are either resistant or intolerant to statins, and that statin efficacy might diminish with patient age in the primary prevention of CVD [2]. Moreover, individuals using statins in clinical practice may be at a higher risk for hyperglycemia, insulin resistance (IR) and eventually type 2 diabetes [3]. In addition, there remains a residual CVD risk, despite these existing treatments being effective for governing plasma LDL-C concentration. These factors suggest that there is an urgent need for new lipid-modulating therapies or independent LDL-C-lowering therapies.

*Co-first authors.

Received: 06 October 2019
Revised: 17 February 2020
Accepted: 21 February 2020

Accepted Manuscript online: 24 February 2020
Version of Record published: 04 March 2020

Clinical Science (2020) **134** 439–458
https://doi.org/10.1042/CS20191028

Recently, sphingolipids have garnered particular attention among the myriad of lipids involved in hyperlipidemia and CVD [4,5]. Ceramides are key precursors in the *de novo* synthesis of sphingomyelin (SM) and glycosphingolipids. Experimental studies have proved that suppressing the generation of sphingolipids, for example by administering serine palmitoyltransferase (SPT) inhibitors, improved glucose and lipid metabolism and alleviated murine atherosclerosis [6,7]. SPT is served as the first enzyme involved in ceramide biosynthesis. The most commonly used SPT inhibitor is thermozymocidin, also known as myriocin, which was originally obtained from a fungus called *Isaria sinclairii*, and used in traditional Chinese medicine [8]. Glycosphingolipids, metabolically downstream of ceramides, have also been implicated as potentially atherogenic lipids. Controversy remains as to whether the inhibition of glycosphingolipid synthesis *per se* has any anti-atherogenic effect [9–11]. An analog of glucosylceramide, D-threo-1-phenyl-2-decanoylamino-3-morpholino-1-propanol (D-PDMP) acts as a glycosphingolipid inhibitor [10]. Both myriocin and D-PDMP show potential for the treatment of atherosclerosis, but their therapeutic efficacy is yet to be evaluated. The underlying mechanisms of their action have also not been fully elucidated.

Here, we systematically evaluated for the first time the role of myriocin, D-PDMP and atorvastatin in metabolic dysfunction and compared their efficacy in reversing atherosclerosis in apolipoprotein E-deficient (apoE$^{-/-}$) mice. To avoid dose deficiency affecting their efficacy, all three drugs were used at their dosage of maximum potency. We observed that myriocin and D-PDMP were almost as effective as atorvastatin in inhibiting the progression of atherosclerotic lesions. Atorvastatin demonstrated the most pronounced effect for lowering serum cholesterol levels because the liver LDL receptors (LDLRs) were markedly up-regulated; this plays a key role in eliminating circulating LDL [12]. In contrast, the sphingolipid inhibitors did not significantly alter cholesterol metabolism in the liver. We assumed that sphingolipid inhibitor-induced smaller plaque sizes may be largely attributed to reduced vascular lipid uptake and/or more cholesterol efflux, rather than reduced serum cholesterol levels. Sphingolipid inhibitors may provide an alternative treatment option for patients whose lipid levels remain elevated despite receiving optimum statin therapy.

Material and methods

Animals and treatments

All animal experiment protocols were approved by the Animal Care and Use Committee of the Peking University First Hospital (J201818) and performed in accordance with all relevant ethical regulations. Male apoE$^{-/-}$ mice (C57BL/6J background, Supplementary Figure S1A) were purchased from Beijing Vital River Laboratory Animal Technology Company (SCXK 2016-0006). A high-fat diet (HFD; 0.15% cholesterol and 21% fat; 4.55 kcal/g) was obtained from Beijing Keao Xieli Feed Company (SCXK 2014-0010). The animal work took place in the animal laboratory of Peking University First Hospital.

Starting at week 12, mice were placed on an HFD and randomly assigned to independent cohorts: (i) vehicle group (n=9), (ii) myriocin group (n=9), (iii) D-PDMP group (n=9) and (iv) atorvastatin group (n=9) (Figure 1A). In the vast majority of cases, patients in need of anti-atherosclerotic therapy already had established atherosclerotic plaques. Thus, the 12-week time-point was chosen for the start of treatment as we found that lipid accumulation had occurred in the aortic sinuses (Supplementary Figure S1B). We aimed to examine the effects of different drugs on atheroma progression. The drugs were administered orally (daily gavage) from weeks 12 to 24, concurrently with the HFD.

Reagents

Myriocin, D-PDMP and atorvastatin were purchased from Sigma–Aldrich (St. Louis, MO, U.S.A.), Matreya LLC (Pleasant Gap, PA) and Pfizer Ltd. (New York, NY, U.S.A.), respectively. The drugs were dissolved in phosphate-buffered saline (PBS) with 5% Tween-80.

Antibodies and dilutions are listed in Supplementary Table S1.

Flow cytometry analysis of blood leukocytes

We collected seven to eight drops of tail blood into 400 μl cold PBS in EDTA-containing tubes. Cell suspensions were stained with anti-CD115–APC, anti-Ly-6c–PE and anti-CCR2–FITC antibodies for 30 min. Then, 600 μl of OptiLyse C Lysing Solution (A11895, Beckman Coulter, Kraemer Boulevard Brea, CA, U.S.A.) was added. The cells were washed twice with PBS followed by centrifugation at 1500 rpm. After being resuspended in 200 μl PBS, the samples were analyzed using a FACSCalibur™ flow cytometer (BD Biosciences, Franklin Lakes, NJ, U.S.A.). Isotype controls were set up and monocytes were gated within a CD115-positive population. CD115-positive and Ly-6c^{high} monocytes were further analyzed for chemoattractant cytokine receptor 2 (CCR2) expression. The data were processed using FlowJo (Tree Star, Ashland, OR, U.S.A.).

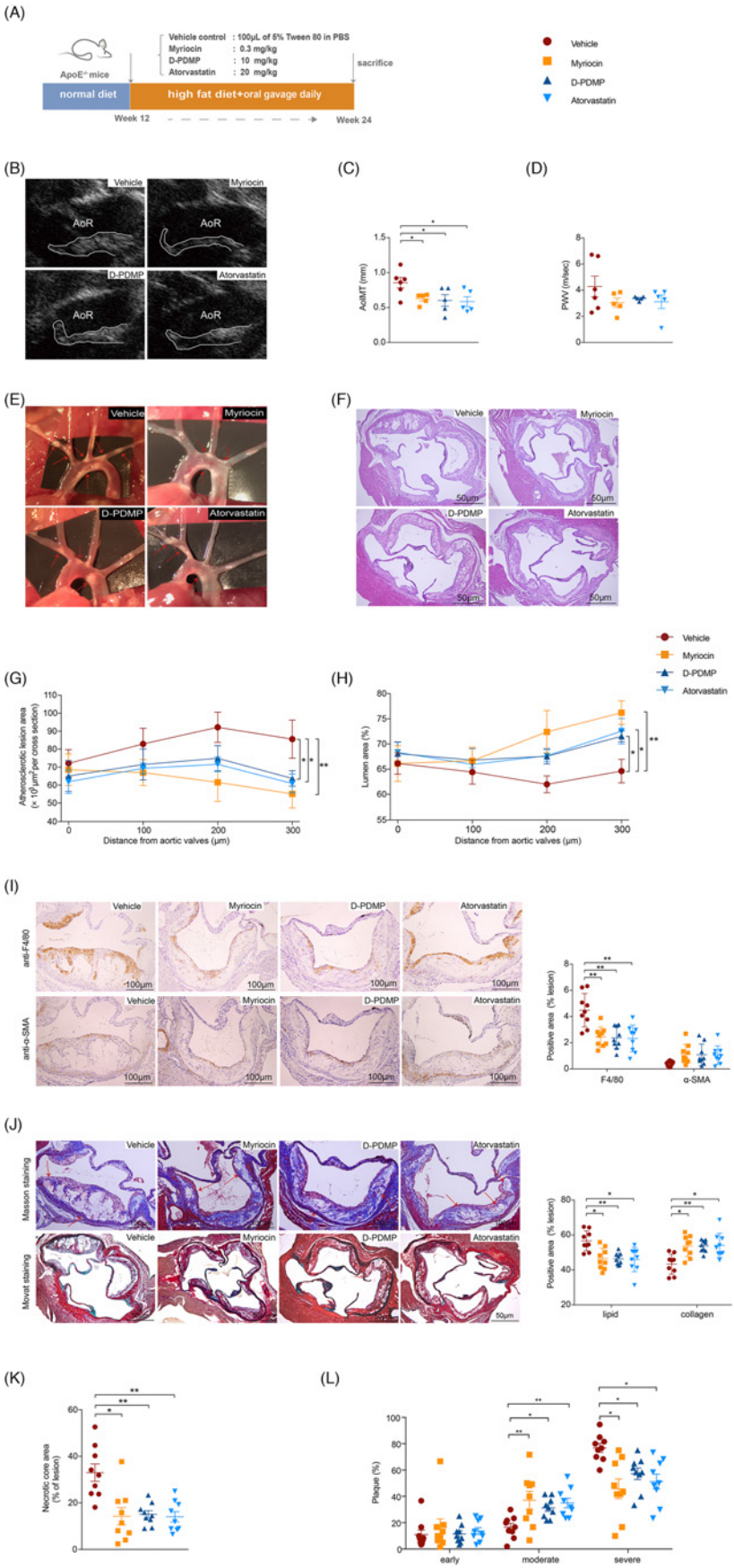

Clinical Science (2020) **134** 439–458
https://doi.org/10.1042/CS20191028

Figure 1. Assessment of atherosclerosis progression in apoE$^{-/-}$ mice following treatment with myriocin, D-PDMP or atorvastatin

(**A**) Experimental design in apoE$^{-/-}$ mice treated with vehicle, myriocin, D-PDMP or atorvastatin. (**B**) Aortic ultrasound imaging. (**C**) Quantitation of aortic intima-media thickness (AoIMT); n=5–6. (**D**) Quantitation of pulse wave velocity (PWV); n=5–6. (**E**) Aortic arches with atherosclerotic plaques (red arrows). (**F**) H&E staining of atherosclerotic lesions in cross-sections of aortic root. Scale bar = 50 μm. (**G**) Quantitative analyses of lesion areas. Image-Pro Plus was used; n=9. (**H**) Quantitative analyses of lumen cross–sectional areas; n=9. (**I**) Immunohistochemical staining of macrophage and smooth muscle cell (SMC) accumulation in lesions (F4/80; α-SMA; brown-stained regions). Scale bar = 100 μm. The bar graph on the right represents quantification data; n=9. (**J**) The top panel represents Masson's Trichrome staining (scale bar = 100 μm) and the bottom panel represents Movat staining (scale bar = 50 μm). The bar graphs on the right represent quantification data of lipid and collagen content; n=9. (**K**) The bar graph shows quantification of necrotic core areas, which were calculated from Masson-stained aortic root sections (red arrows); n=9. (**L**) The distribution of early, moderate and advanced plaques based on histological staging of the atherosclerotic lesions; n=9. All data are expressed as means ± SEM. Statistical significance was determined by one-way ANOVA. $^{*}P<0.05$ was considered significant, $^{**}P<0.01$. Abbreviation: H&E, Hematoxylin and Eosin.

Ultrasound imaging

Mice were anesthetized with 1.5% isoflurane and then placed in supine position on a temperature- and electrocardiogram (ECG)-controlled plate. During the measurement process, the animals were maintained at a normal physiological heart rate of approximately 450 beats/min. M-mode echocardiograms were obtained in the parasternal long-axis view and short-axis view of the left ventricle at the level of the papillary muscles using an ultrasound imaging system (Vevo770, Visualsonics Inc., Toronto, Canada). For each mouse, five cardiac cycles were used for measurement.

Intima-media thickness (IMT) was measured in the ascending aorta long-axis view and pulse wave velocity (PWV) measurement was performed in the aortic arch long-axis view. The PWV was calculated by dividing D (the thoracic–abdominal distance) by T (the pulse transit time). Pulse transit time was determined by the time delay between the feet of the proximal and distal aortic flow-waves in reference to the R wave of the ECG.

Oral glucose tolerance test

Forty-eight hours prior to the mice being killed, oral glucose tolerance test (OGTT) was performed. The mice were fasted for 16 h to exhaust their liver glycogen and minimize blood glucose variability. Glucose was then orally administered at a dosage of 2 g/kg body mass. Blood glucose levels were measured at 0, 15, 30, 60 and 120 min using a glucometer (Sinomedisite, Beijing, China). The area under the curve (AUC) was calculated using the trapezoidal method.

Additional blood samples (20 μl) for the determination of insulin levels were collected at baseline. An Ultra-Sensitive Mouse Insulin ELISA kit (Crystal Chem, Downers Grove, IL, U.S.A.) was used, following the manufacturer's instructions. Whole-body IR was estimated using the homeostatic model assessment (HOMA)-IR index. HOMA-IR = fasting insulin level (IU/ml) × fasting glucose level (mg/dl)/405.

Biochemical analysis

Blood samples were collected following an overnight starvation period. Serum total cholesterol (TC), LDL-C, high-density lipoprotein-cholesterol (HDL-C), triglyceride (TG), alanine aminotransferase (ALT) and aspartate aminotransferase (AST) concentrations were measured using an automated analyzer (Beckman, Brea, CA, U.S.A.). High-sensitivity C-reactive protein (hs-CRP) was measured using an enhanced immunoturbidimetric assay.

The quantification of mouse adiponectin in serum was analyzed using a high-quality enzymatic assay kit (Crystal Chem, Downers Grove, U.S.A.). The serum level of oxidized LDL (ox-LDL) was measured using a commercial mouse ox-LDL ELISA kit (Cloud Clone Corp, Wuhan, China).

HPLC analysis of serum sphingolipid levels

For lipid extraction, 300 μl of Folch solution (chloroform/methanol, 2:1, v:v) and 10 μl internal standard mixture was added to 75 μl mouse serum. Then, the samples were vortexed for 30 s and centrifuged at 14000 rpm for 15 min. The chloroform layer was collected and dried with nitrogen. Finally, the lipid extracts were redissolved in 150 μl Folch solution.

A CORTECS C18 column (2.1 × 100 mm, 2.7 μm particle size, 90 Å pore size; Waters, Milford, MA, U.S.A.) was used for lipid separation. The mobile phases A and B were acetonitrile/water (60/40) with 10 mM ammonium acetate

(mobile phase) and acetonitrile/isopropanol (10/90), respectively. The gradient was set as follows: 0—1.5 min, 37% to 37% B; 1.5—4 min, 37% to 45% B; 4—5 min, 45% to 52% B; 5—8 min, 52% to 58% B; 8—11 min, 58% to 66% B; 11—14 min, 66% to 70% B; 14—18 min, 70% to 75% B; 18—20 min, 75% to 98% B; 20—22 min, 98% to 98% B; 22—22.1 min, 98% to 37% B; 22.1—25 min, 37% to 37% B.

Qualitative and quantitative analyses were performed using a Q Exactive Orbitrap mass spectrometer (Thermo Scientific, CA, U.S.A.). A full-scan spectrum was recorded over the 240–2000 m/z range, and the qualitative assignment of sphingolipids was carried out in the MS/MS mode. Detailed parameters were as follows, source temperature: 320°C, sheath gas flow rate: 35 arb, aux gas flow rate: 10 arb, full scan resolution: 70000; MS/MS resolution: 17500. The resulting data were analyzed using LipidSearch 4.1.30 (Thermo Scientific, CA, U.S.A.). The mass tolerances of precursor and fragment ions were 5 and 10 ppm, respectively.

Liver histology

Following euthanasia, mice were perfused with 10 ml of ice-cold normal saline. The livers were dissected and weighed. The middle lobes of livers were embedded in optimum cutting temperature compound (OCT) (Sakura, Tokyo, Japan) and 7-μm-thick cryosections were stained with Hematoxylin and Eosin (H&E; Beyotime, Shanghai, China) and Oil Red O (Solarbio, Beijing, China). The lipid contents of livers were quantified using Image-Pro Plus (IPP) software (Media Cybernetics, Bethesda, MD, U.S.A.).

Hepatic TG content

Pieces of liver (100 mg) were homogenized in absolute ethyl alcohol within an ice-water bath. TG concentrations in livers were measured using commercial kits (Nanjing Jiancheng Bioengineering Institute, Nanjing, China), according to the manufacturer's protocols.

Assessment of oxidative stress in liver

Liver tissue samples (approximately 100 mg) were sonicated and homogenized in normal saline on ice. Oxidative stress markers were measured using a total antioxidant capacity (T-AOC) assay kit, a micro-reduced glutathione (GSH) assay kit, a superoxide dismutase (SOD) assay kit (WST-1 method), a catalase (CAT) assay kit (Ultraviolet), and a malondialdehyde (MDA) assay kit (TBA method). All kits came from Nanjing Jiancheng Bioengineering Institute, China.

Histological evaluation of atherosclerotic lesions

The aortic arches were carefully isolated under a stereo microscope (Leica, Wetzlar, Germany) and photographed. The entire aortas were then dissected and fixed in 4% paraformaldehyde. Before being stained with Oil Red O for *en face* analysis, periadventitial fat and connective tissue were carefully removed using microforceps and microscissors. For the photography, the whole aorta was opened longitudinally and pinned to a black cystosepiment surface.

For the aortic sinus analysis, aortic roots were dehydrated and embedded in paraffin. Starting from the appearance of the aortic valve, sequential sections 4-μm-thick were collected across the aortic root (approximately 350 μm in total). For each mouse, sections of 100-μm-intervals were used to evaluate the size of atherosclerotic lesions. The severity of plaques was classified as: early lesions, with early fatty streaks; moderate lesions, with a collagenous cap; and advanced lesions, with an increased necrotic area and involvement of the media. Morphological analysis of collagen contents in the lesions was performed by staining with Movat Pentachrome. The lipid area was defined as Masson's trichrome stain-free. Images were captured under a Nikon Eclipse Ti2 microscope (Kyoto, Japan). Plaque necrotic core areas were manually drawn. Quantification was completed using IPP software.

Immunohistochemistry

For macrophage and smooth muscle cell (SMC) area quantification, we selected cross-sections at the same level where the three aortic valve leaflets appeared simultaneously. The sections were incubated with primary antibodies, followed by horseradish peroxidase (HRP)-conjugated secondary antibodies (Supplementary Table S1), and then developed using DAB substrate (brown).

Immunofluorescence staining

Briefly, the sections of aortic root were blocked in PBS with the appropriate serum (10%) for 1 h, incubated at 4°C overnight with primary antibodies, and then stained with fluorescent-dye-conjugated secondary antibodies for 1 h

Clinical Science (2020) **134** 439–458
https://doi.org/10.1042/CS20191028

at 37°C (Supplementary Table S1). Mounting medium with DAPI (ZSGB-Bio, Beijing, China) was used to stain the nuclei. Images were captured and processed using identical settings in a Nikon A1MP inverted confocal microscope.

Quantitative real-time PCR

Total RNAs of snap-frozen liver or aorta tissue were isolated using TRIzol Reagent (Life Technologies, Carlsbad, CA, U.S.A). Reverse transcription was performed with a TransScript First-Strand cDNA Synthesis kit (TransGen Biotech, Beijing, China). The real-time PCR reaction system (20 μl volume) was prepared by mixing cDNAs, TransStart Top Green qPCR Super Mix (TransGen) and gene-specific primers which are listed in Supplementary Table S2. PCR amplification consisted of an initial denaturation step at 95°C for 10 min, followed by 40 cycles of PCR at 94°C for 5 s and 60°C for 40 s (CEX Connect Real-Time System, Bio-Rad, Hercules, CA, U.S.A.). Quantification of relative mRNA expression was calculated using the efficiency-corrected $2^{-\Delta\Delta CT}$ method. Actin gene expression was used as the internal control, and the differences were presented as fold-changes relative to the vehicle group.

Western blotting analyses

Mouse tissue proteins were extracted using RIPA lysis buffer (Applygen, Beijing, China) supplemented with 1% protease and 1% phosphatase inhibitors (Roche, Mannheim, Germany). The samples were sonicated for several seconds on ice and then centrifuged for 15 min at 15000 rpm. We collected samples of the supernatants and quantified the proteins using a BCA assay kit (Pierce, Rockford, IL, U.S.A.). The samples were then boiled for 5 min with loading buffer added.

For separation, the samples were loaded on to a 10% SDS/PAGE gel (Genscript, Nanjing, China) at 30–40 μg per lane. The proteins were then transferred to polyvinylidene difluoride membranes (Millipore, Bedford, MA). After blocking with 5% non-fat dried milk, the membranes were incubated with primary antibodies overnight at 4°C, and then with appropriate secondary antibodies at room temperature for 1 h. Blots were detected using a chemiluminescence detection system (G:BOX Chemi XT4, Syngene) and viewed in ImageJ software for data analysis. All protein levels were normalized to β-actin or α-tubulin signals. Uncropped scans of Western blots are provided in Supplementary Figures S2 and S3.

Statistical analyses

Statistical analyses were performed using SPSS v.22.0 software (IBM Corp., Armonk, NY, U.S.A.). All continuous variables were presented as the mean ± SEM and statistical significance was accepted when $P<0.05$. One-way ANOVA followed by a least significant difference (LSD) post hoc test (equal variances assumed) or Dunnett's post hoc test (no equal variances assumed) was applied for comparisons among the groups.

Pearson's chi-squared test was used to verify the correlation between certain sphingolipids and the intervention compounds. Then the correlations were calculated by Spearman's rank correlation coefficient. Any test results reaching a liberal statistical threshold of $P<0.2$ for each comparison were then entered multivariable linear regression model. At last, we conducted univariate logistic regression analyses to explore associations between some specific glycosphingolipid and drug.

Results

Assessment of atherosclerosis progression in apoE$^{-/-}$ mice following treatment with myriocin, D-PDMP or atorvastatin

Myriocin-treated, D-PDMP-treated, atorvastatin-treated and vehicle-control mice were fed on a HFD for 12 weeks (Figure 1A). Myriocin and D-PDMP were well-tolerated and caused no overt side effects. One animal in the atorvastatin group exhibited hair loss, low body mass and abnormal splenomegaly. At the end of week 24, we performed mouse trans-thoracic echocardiography. Heart function was measured and the ejection fraction and fractional shortening were found to be comparable among the four groups (Supplementary Table S3 and Figure S4A–C). The left ventricular mass was reduced in the D-PDMP group compared with the vehicle and atorvastatin groups (Supplementary Figure S4D). Vascular ultrasound studies revealed that aortic intima thickening was noticeably reduced following treatment with myriocin, D-PDMP and atorvastatin, compared with the vehicle group (Figure 1B,C). PWV measurements, reflecting vascular stiffness, revealed a similar pattern (Figure 1D). We photographed the aortic arches and dissected the aortas (Figure 1E and Supplementary Figure S4E). One aorta from each group was randomly selected for Oil Red O staining (Supplementary Figure S4F).

To quantify the degree of lumen stenosis, aortic-root sections were stained with H&E, Figure 1F). We found that all mice (36 of 36) had lesions in their aortic roots; however, the lesions in the myriocin-, D-PDMP- and

atorvastatin-treated mice were smaller than those of mice treated with vehicle (−35.6%, $P<0.01$; −25.6%, $P<0.05$; −28.9%, $P<0.05$, respectively; Figure 1G). Additionally, the lumen cross-sectional areas were larger in the treatment groups compared with the control (Figure 1H). Similar observations were made with cross-sections of the ascending aorta (Supplementary Figure S4G). Notably, myriocin seemed to show better efficacy than atorvastatin.

Next, a more detailed analysis of aortic-root plaque composition was performed. We found that the three groups of drug-treated mice showed a significant reduction in macrophage content compared with the vehicle-control mice group, as determined by immunostaining of F4/80 cell-surface glycoproteins (myriocin, −45.3%, $P<0.01$; D-PDMP, −49.3%, $P<0.01$; atorvastatin, −44.4%, $P<0.01$; Figure 1I). No significant differences were seen by staining for α-SMA, a biomarker of SMCs (Figure 1I). Fewer lipid areas were observed in the plaques but their collagen content was increased by treatment with myriocin, D-PDMP and atorvastatin (Figure 1J). The necrotic core areas, which are features of vulnerable plaques, showed significant reduction (Figure 1K). On the basis of these results, it was shown that mice receiving drug treatment displayed more early-to-moderate lesions, with fewer severe lesions (Figure 1L).

Effects of myriocin, D-PDMP and atorvastatin on hyperlipidemia in apoE$^{-/-}$ mice

Following myriocin, D-PDMP and atorvastatin treatment, we evaluated the ability of these drugs to lower the serum lipid concentration and improve the lipid profile. Compared with the vehicle group, treatment with atorvastatin decreased the serum levels of TC, LDL-C, VLDL-C and free fatty acids (FFA, Figure 2A). Slightly decreased levels of LDL-C were observed in the myriocin-treated group. Unexpectedly, treatment with D-PDMP neither significantly lowered serum TG, TC, LDL-C or VLDL-C, nor did it increase HDL-C levels (Figure 2A,B). This result was consistent with an earlier finding by Garner et al. that treatment with another glycosphingolipid inhibitor, EtDO-P4, did not elicit significant changes in plasma TC or TG levels [9]. However, our results were inconsistent with those of Chatterjee et al. [10], who found that treatment with D-PDMP significantly decreased LDL-C (∼70%) and TG (∼50%) and increased HDL-C (approximately three-times). There are several possible explanations which could account for these differences. First, both our group and Garner et al. fed mice an HFD (0.15% cholesterol), whereas Chatterjee et al. [10] fed mice a Western-style diet (1.25% cholesterol). The TG levels (∼790 mg/dl) in vehicle group from Chatterjee et al.'s [10] data were obviously higher than the levels in the present study (∼100 mg/dl) and Garner et al.'s study (∼140 mg/dl). Second, Chatterjee et al. [10] treated their apoE$^{-/-}$ mice for 24 weeks, twice the duration of drug treatment in our study. In addition, the lower TG in our study may be partially related to fasting state, as prolonged fasting reduced TG levels.

The effects of the various treatments on the serum sphingolipidome were determined by Orbitrap-based high throughput metabolomics analysis. Sphingolipid metabolism involves a vast, complex network. Briefly, once ceramides have been generated they are converted into complex sphingolipids, such as SMs, glucosyl-ceramides (monohexosylceramides), lactosyl-ceramides (dihexosylceramides) and GM3 gangliosides. SMs and glycosphingolipids are involved in the hydrolytic pathway of ceramide metabolism [13]. Previous studies have demonstrated that treatment with myriocin can decrease the level of all sphingolipids in rodent models, including ceramides, SMs and glycosphingolipids [6]. However, we observed that treatment with myriocin resulted in serum levels of total ceramides that were comparable with those in the vehicle-control group (Figure 2C). The total SM level was significantly decreased by both myriocin and atorvastatin treatment (−11.0 and −13.5%, respectively; $P<0.05$, Figure 2G). Given that serum SM is a component of lipoprotein particles, this may partly explain the reduction in serum LDL-C. Moreover, the data showed the levels of which particular sphingolipids were altered (Figure 2D–I). Multivariate linear regression analysis identified C16-dSM as the most altered one (Supplementary Table S4A,B). In the present study, we also found that D-PDMP impeded the conversion of ceramides into glycosphingolipids (−12.2%, $P<0.05$; Figure 2J,K). Univariate logistic regression analysis verified that D-PDMP lowered serum dHex1Cer (Supplementary Table S5A–C). Serum ceramides were simultaneously elevated by D-PDMP, although this was not statistically significant compared with the vehicle group, which may partially compromise the beneficial effects brought about by D-PDMP. When considered in concert, the studies suggest that, compared with atorvastatin, sphingolipid inhibitors show a relatively minor efficiency for lowering lipid levels in blood.

Effects of myriocin, D-PDMP and atorvastatin on hepatic lipid metabolism

To investigate how the different treatments affected lipid metabolism, we first tested their liver histopathology. As expected, none of the interventions significantly affected the level of hepatocyte damage-markers (AST and ALT) in peripheral blood (Figure 3A,B). However, the mass of the livers in myriocin-treated mice unexpectedly increased compared with mice in the control group and the atorvastatin-treatment group (Figure 3C–E). Histologically, liver

Clinical Science (2020) **134** 439–458
https://doi.org/10.1042/CS20191028

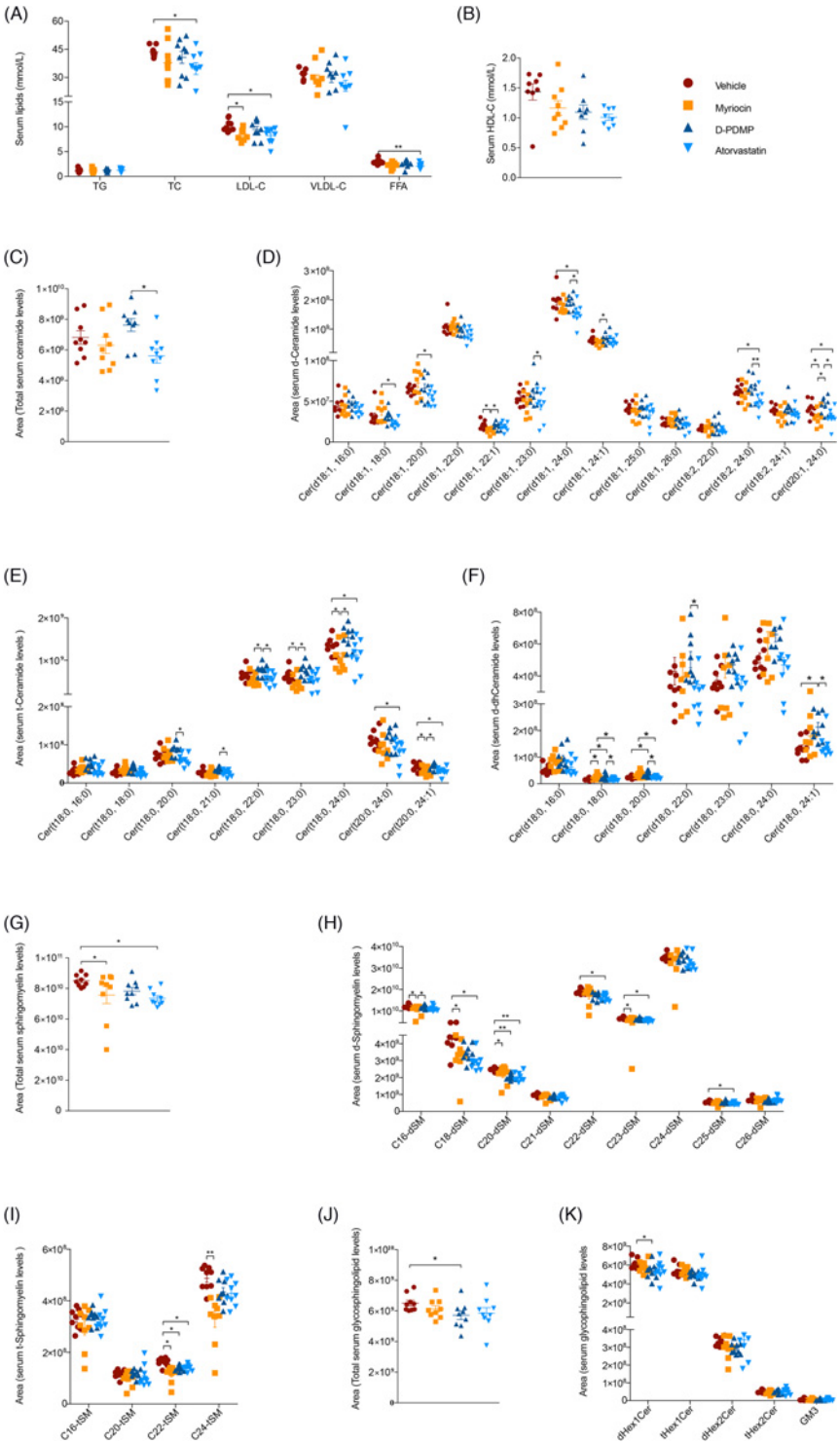

Figure 2. Effects of myriocin, D-PDMP and atorvastatin on hyperlipidemia in apoE$^{-/-}$ mice

(**A**) Circulating TG, TC, LDL-C, very LDL-C (VLDL-C) and FFA levels; n=8–9. (**B**) Circulating HDL-C level; n=8–9. (**C**) Total serum ceramide species levels were quantified; n=9. (**D**) Analysis of serum d-ceramide species (d means the sphingoid base is sphingosine); n=9. (**E**) Analysis of serum t-ceramide species (t means the sphingoid base is phytosphingosine); n=9. (**F**) Analysis of serum d-dhceramide (d-dihydroceramide) species; n=9. (**G**) Total serum SM species levels were quantified; n=9. (**H**) Analysis of serum d-SM species; n=9. (**I**) Analysis of serum t-SM species; n=9. (**J**) Total serum glycosphingolipid species levels were quantified; n=9. (**K**) Analysis of serum glycosphingolipid species; n=9. All data are expressed as means ± SEM. Statistical significance was determined by one-way ANOVA. *P<0.05 was considered significant, **P<0.01.

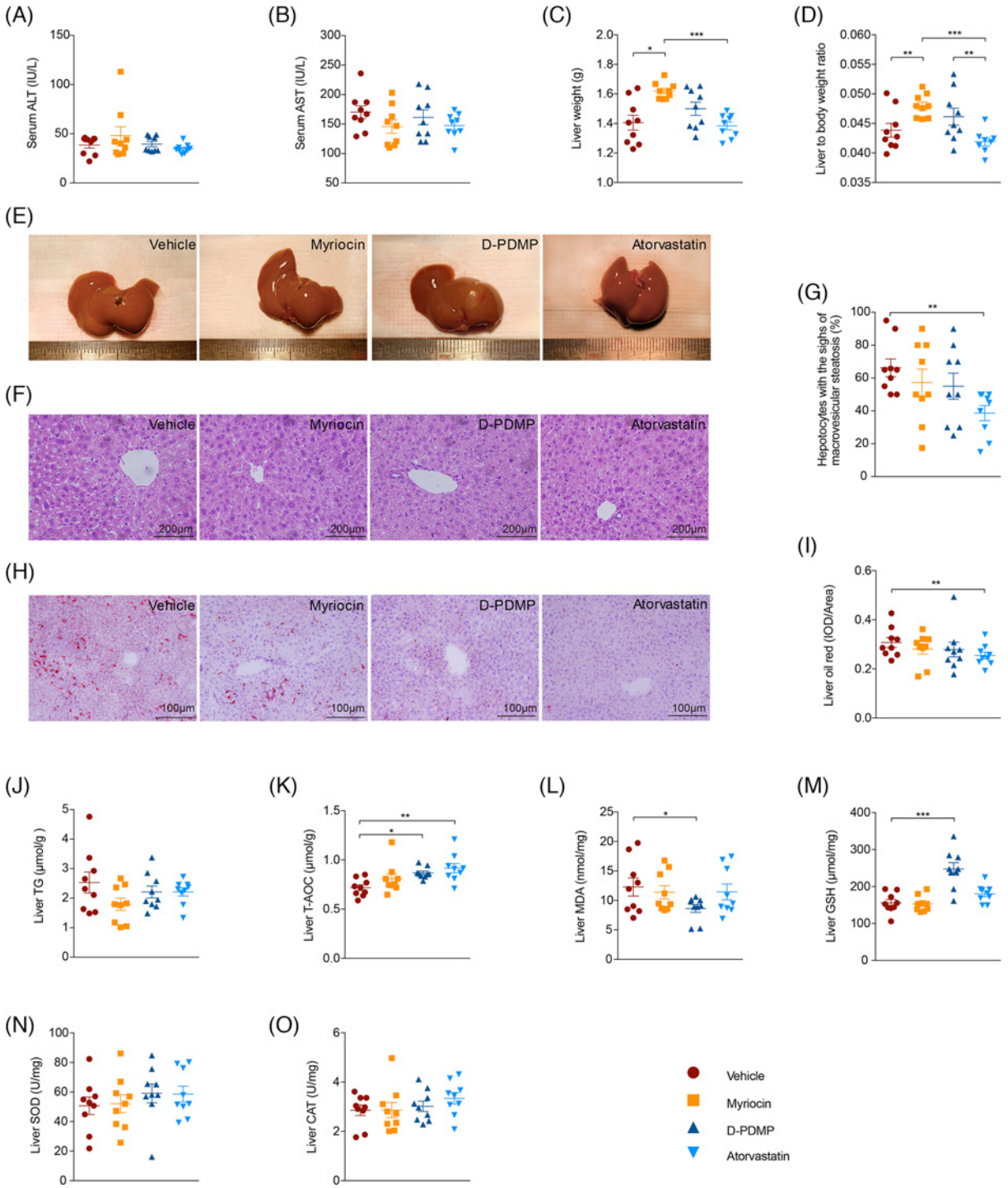

Figure 3. Effects of myriocin, D-PDMP and atorvastatin on hepatic lipid accumulation in apoE$^{-/-}$ mice

(**A**) Serum ALT level; n=9. (**B**) Serum AST level; n=9. (**C**) Liver masses. n=8–9. (**D**) The masses of the livers, normalized to the total body mass of the mice. n=8–9. (**E**) A representative gross image of a liver. (**F**) Representative H&E-stained images of vehicle-, myriocin-, D-PDMP- and atorvastatin-treated livers. (**G**) Quantification of hepatocytes with signs of macrovesicular steatosis; n=9. (**H**) Representative images of Oil Red O staining of livers. (**I**) Quantification of liver lipids stained by Oil Red O; n=9. (**J**) Quantification of TG content in livers; n=9. (**K**) T-AOC in liver tissues; n=9. (**L**) MDA levels in liver tissues; n=9. (**M**) GSH levels in liver tissues; n=9. (**N**) SOD activity in liver tissues; n=9. (**O**) CAT activity in liver tissues; n=9. All data are expressed as means ± SEM. Statistical significance was determined by one-way ANOVA. $^{*}P<0.05$ was considered significant, $^{**}P<0.01$, $^{***}P<0.001$.

Clinical Science (2020) **134** 439–458
https://doi.org/10.1042/CS20191028

samples from the atorvastatin-treated mice exhibited the lowest intrahepatocyte lipid-droplet storage and the mildest disorganization of hepatic chord architecture (Figure 3F–J). Although it has been reported that the use of genetic engineering approaches or specific inhibitor treatments to decrease sphingolipids could reverse hepatic steatosis in obese rodents [14,15], these findings were not observed in our study. Atorvastatin treatment appears to be the most effective for attenuating hepatic lipid accumulation in apoE$^{-/-}$ mice.

Next, we performed an analysis of mRNAs involved in cholesterol metabolism (Hmgr, Ldlr, Pcsk9, Srebp2 and Acat1; Figure 4A), fatty-acid uptake (Cd36, Fabp1 and Caveolin-1; Figure 4B), cholesterol efflux (Abca1, Apoa1, Abcg1, Abcg5, Abcg8 and Cyp7a1; Figure 4C), TG metabolism (Lpl and Vldr; Figure 4D), fatty-acid synthesis (Lxra, Lxrβ, Srebp-1c, Fas, Acc and Scd-1; Figure 4E) and oxidation (Pparα, Acs1, Cpt1a, Acox1 and Cyp4a1; Figure 4F). Mice treated with atorvastatin exhibited the anticipated up-regulated expression of the hepatic *Ldlr* gene, consistent with the reduced levels of serum cholesterols. A reduction in the expression of genes involved in fatty-acid uptake and synthesis pathways was evident in both the myriocin- and D-PDMP-treated groups (Figure 4B,E). Western blot analyses confirmed the reductions in cluster of differentiation 36 (CD36), Caveolin-1 and SCD-1 proteins (Figure 4G,H,J). Although some studies have suggested that myriocin can reduce serum TG and that D-PDMP plays a role in promoting cholesterol efflux and TG metabolism [6,10], we found no evidence to support these claims in the present study (Figure 4C,D,I). The promotion of fatty-acid oxidation was seen in atorvastatin-treated mice (Figure 4F).

Taken together, these findings suggest that sphingolipid inhibitors do not significantly affect cholesterol metabolism and that their protective role in fatty-acid metabolism is not sufficient to reverse liver lipid-deposition. These results also hinted that the main mechanism linking sphingolipid inhibitors to decreased atherosclerosis in apoE$^{-/-}$ mice is probably not involved in the hepatic clearance of excessive lipids but may instead be involved in vascular lipid uptake or other pathways.

Inhibition of sphingolipid synthesis ameliorates vascular lipid accumulation via mechanisms involving the reduction in Ly-6c^{high} monocytes and vascular scavenger receptors

Here, we sought to understand the main contribution of these strategies (myriocin and D-PDMP) to reducing lipid accumulation. Before macrophages bind and internalize ox-LDL, circulating monocytes are recruited and then the arterial intima is entered. Recent observations have indicated that Ly-6c^{high} monocytes show a greater capacity to form foam cells compared with Ly-6c^{low} cells [16]. We performed flow cytometry analysis of peripheral blood sampled at weeks 16, 20 and 24. At the end of week 20, we found that monocytes from vehicle-treated apoE$^{-/-}$ mice were predominantly of the Ly-6c^{high} phenotype, whereas cells of this phenotype were significantly decreased by myriocin, D-PDMP or atorvastatin (−19.4%, $P<0.05$; −23.5%, $P<0.01$; −24.4%, $P<0.01$, respectively; Figure 5A,B). Furthermore, also at the end of week 20, CCR2-positive monocytes were down-regulated compared with control mice (myriocin, 28.1%, $P<0.01$; D-PDMP, −40.0%, $P<0.001$; atorvastatin, −40.0%, $P< 0.001$; Figure 5C,D). This receptor plays a critical role in the migration of monocytes. Its primary ligand, monocyte chemotactic protein 1 (MCP-1), was detected by immunofluorescence staining in sections of atherosclerotic lesions, showing correspondingly lower levels in myriocin, D-PDMP and atorvastatin group (Figure 5E).

Following the trafficking of monocytes into arteries, these cells form foamy macrophages. This process is controlled by three pathways: the influx of modified lipoproteins, the biosynthesis of cholesteryl ester, and lipid efflux [17]. We tested aorta tissues for the markers representing these pathways. As anticipated, in atorvastatin-treated mice the expression of scavenger receptors, such as the lectin-like ox-LDL receptor-1 (LOX-1) and scavenger receptor-A (SR-A), was reduced, in accordance with the reduction in circulating lipids (Figure 5F,J,K). Unlike with atorvastatin treatment, the expression of CD36 was significantly suppressed by myriocin and D-PDMP treatment (Figure 5I). Notably, the expression of LOX-1 was strikingly down-regulated by all treatments at the level of both mRNA and protein, suggesting LOX-1 is a common target for these drugs. Immunofluorescence staining of aortic-root cross-sections showed decreased LOX-1 expression and its colocalization with CD68 (Figure 5P).

No significant difference was observed in the level of expression of ATP-binding cassette transporter G1 (ABCG1), which is responsible for cholesterol efflux, or the enzyme required for cholesterol esterification (ACAT1; Figure 5G,H,M). In addition, the main lipid droplet-coating protein in foam cells, perilipin2, was detected. Perilipin2 has been shown to play an important role in the formation of atheroma [18]. In the present study, the down-regulation of perilipin2 by sphingolipid inhibitors at the mRNA level was significantly compared with vehicle-treated animals, but at the protein level there were no statistically significant differences among the groups (Figure 5N,O).

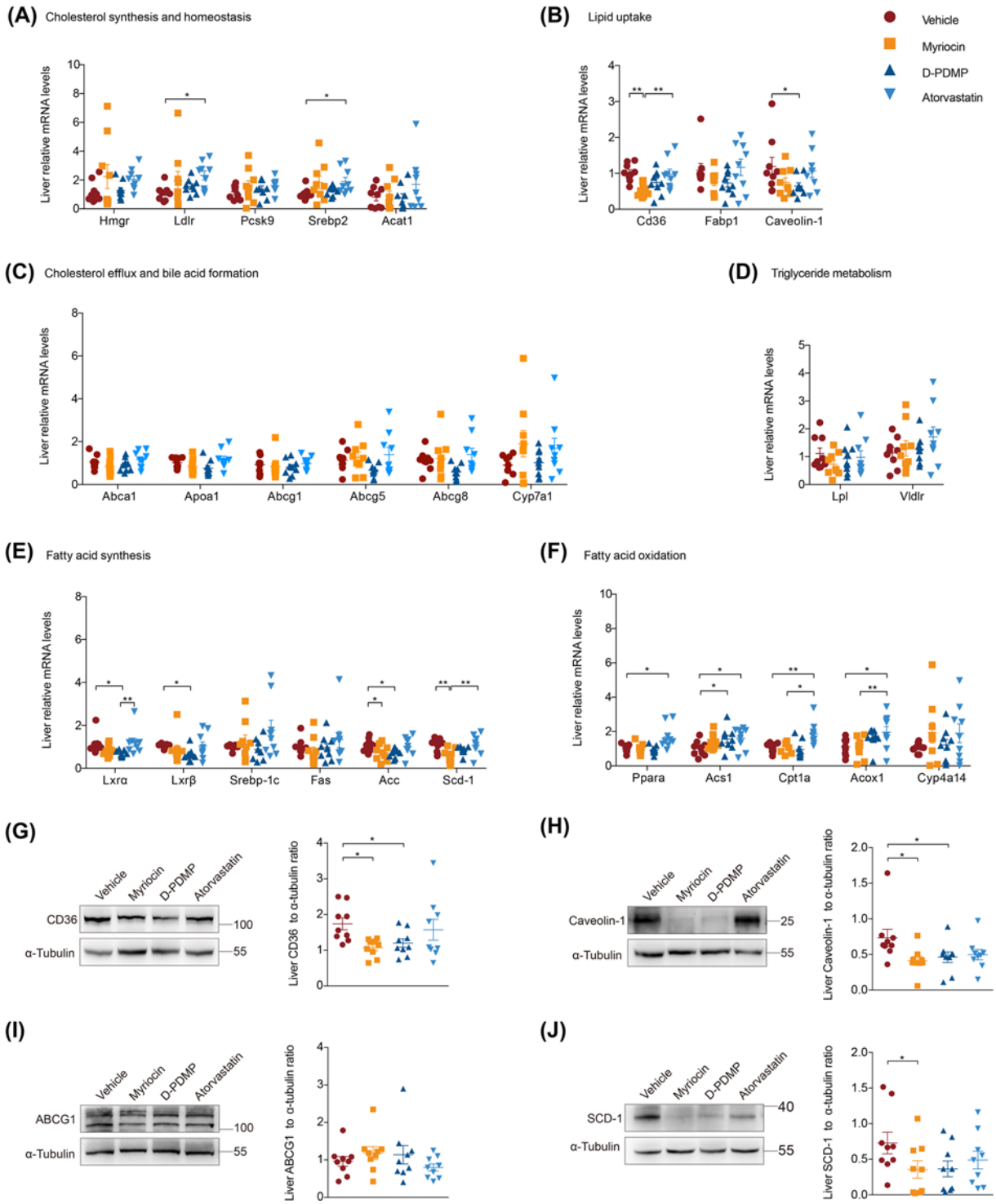

Figure 4. Effects of atorvastatin, myriocin and D-PDMP on hepatic lipid metabolism in apoE$^{-/-}$ mice

(**A**) The relative abundance of hepatic genes involved in cholesterol synthesis and homeostasis was assessed by quantitative PCR; n=9. (**B**) Hepatic genes involved in fatty-acid uptake; n=9. (**C**) Hepatic genes involved in cholesterol efflux and bile acid formation; n=9. (**D**) Hepatic genes involved in TG metabolism; n=9. (**E**) Hepatic genes involved in fatty-acid synthesis; n=9. (**F**) Hepatic genes involved in fatty-acid oxidation; n=9. (**G**) Hepatic expression of CD36 protein was assessed by Western blotting. The bar graphs on the right represent relative protein quantification; n=9. (**H**) Hepatic expression of Caveolin-1 protein; n=9. (**I**) Hepatic expression of ABCG1 protein; n=9. (**J**) Hepatic expression of SCD-1 protein; n=9. α-Tubulin protein was used as loading control. All data are expressed as means ± SEM. Statistical significance was determined by one-way ANOVA. *P<0.05 was considered significant, **P<0.01. Abbreviation: ABCG1, ATP-binding cassette transporter G1.

Clinical Science (2020) **134** 439–458
https://doi.org/10.1042/CS20191028

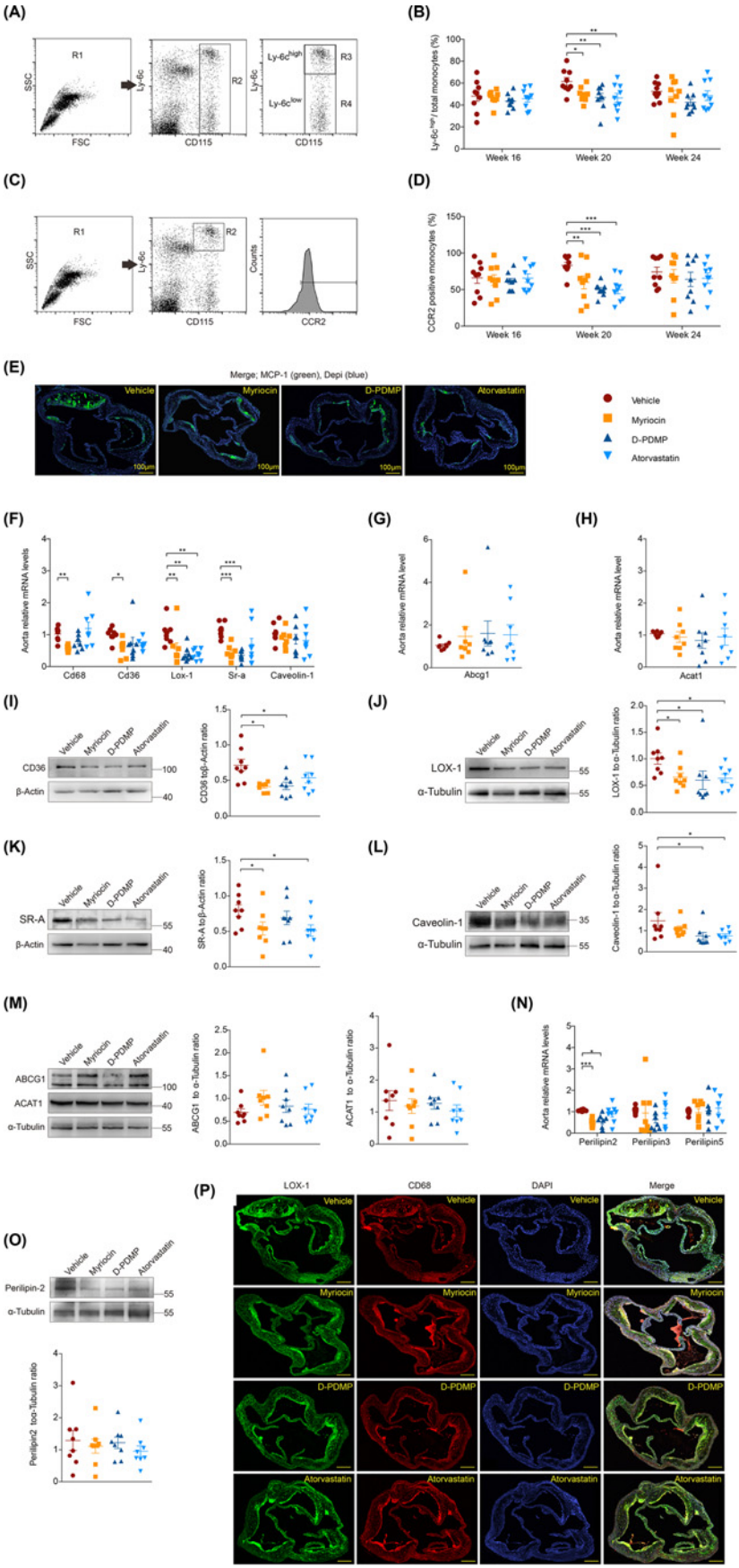

Figure 5. Inhibition of sphingolipid synthesis diminishes the expression of proteins involved in lipid uptake

(**A**) Flow-cytometric analysis of blood monocytes. The left dot-plot shows total Ficoll–Paque fractionated blood cells. Cells gated in region R1 are living, nongranular white blood cells. Region R2 gates monocytes, as indicated by their CD115 expression. Cells gated in regions R3 and R4 are Ly-6c^{high} and Ly-6c^{low} monocytes, respectively. (**B**) Comparison of the percentage of Ly-6c^{high} monocytes (R3 gated cells) among total monocytes (R2 gated cells); n=9. (**C**) Blood CD115^{+}/Ly-6c^{high} cells were further analyzed for CCR2 expression. (**D**) Comparison of the percentage of CCR2-positive cells; n=9. (**E**) Representative images of immunostaining for MCP-1 in aortic-root lesions. (**F**) Relative abundance of aortic Cd68 mRNA, Cd36 mRNA, Lox-1 mRNA, Sr-α mRNA and Caveolin-1 mRNA; n=8. (**G**) Relative abundance of aortic Abcg1 mRNA; n=8. (**H**) Relative abundance of aortic Acat1 mRNA; n=8. (**I**) Aortic expression of CD36 protein; n=8. (**J**) Aortic expression of LOX-1 protein; n=8. (**K**) Aortic expression of SR-A protein; n=8. (**L**) Aortic expression of Caveolin-1 protein; n=8. (**M**) Aortic expression of ABCG1 and ACAT1 proteins; n=8. (**N**) Relative abundance of aortic Perilipin2, Perilipin3 and Perilipin5 mRNA; n=8. (**O**) Aortic expression of Perilipin2 protein. Proteins were examined by Western blotting, and α-Tubulin and β-Actin were used for loading controls, as indicated. (**P**) Immunofluorescence staining for LOX-1 and CD68 in apoE$^{-/-}$ mouse atherosclerotic lesions (LOX-1, green; CD68, red; DAPI, blue). Scale bar = 100 μm. All data are expressed as means $\pm$ SEM. Statistical significance was determined by one-way ANOVA. *P<0.05 was considered significant, **P<0.01, ***P<0.001. Abbreviations: LOX-1, lectin-like ox-LDL receptor-1; SR-A, scavenger receptor-A.

The inflammatory response was commonly compromised by myriocin, D-PDMP and atorvastatin

During the progression of atherosclerosis, foam-cell accumulation induces inflammatory responses, apoptosis and other adverse effects. Numerous studies have demonstrated that atorvastatin attenuates plaque vulnerability by reducing inflammation. Some reports have shown that myeloid cell-specific SPT haploinsufficiency can mitigate inflammatory responses [7], but other reports have suggested that myriocin does not appear to ameliorate the activation of hepatic inflammation [19]. Since little is known about the role of myriocin or D-PDMP in vascular inflammation or apoptosis, we hypothesized that these two inhibitors could improve plaque stability by attenuating the inflammatory signaling cascade.

The circulating concentration of hs-CRP, an inflammatory biomarker, was significantly decreased by both D-PDMP and atorvastatin (Figure 6A). Similar reduction was observed in aortic protein MAC-3, a marker for macrophages (Figure 6B). Myriocin also led to a down-regulated trend, with less hs-CRP and MAC-3. To obtain additional lines of evidence, we next analyzed the expression of genes involved in vascular inflammation. The mRNA levels of pro-inflammatory cytokines (Il-1β, Il-6 and tumor necrosis factor α (Tnf-α)), chemokines (Ccl-2) and adhesion molecules (Icam-1 and Vcam-1) were in general down-regulated by the two inhibitors (Figure 6C). Immunofluorescence staining for IL-1β in atherosclerotic lesions and immunoblotting for the VCAM-1 protein showed a corresponding down-regulation (Figure 6D,E). The marker of angiogenesis, vascular endothelial growth factor (VEGF), showed a similar change at the mRNA level but no significant difference was found at the protein level (Figure 6E). Besides, D-PDMP induced the up-regulation of Il-10, an anti-inflammatory cytokine (Figure 6C). Collectively, myriocin treatment reduced aortic inflammatory responses, while D-PDMP treatment exerted a robust anti-inflammation function, although it could not correct the abnormally high serum cholesterols in apoE$^{-/-}$ mice.

Since myriocin and D-PDMP showed anti-inflammatory properties, we also tested their antioxidative properties, because oxidative stress plays an important role in aggravating atherogenesis. The serum level of ox-LDL was decreased by D-PDMP and atorvastatin, and the level of T-AOC was correspondingly increased (Figure 6F,G). We next investigated aortic mRNA expression of antioxidant enzymes, such as SOD and CAT, and the subunits of NADPH oxidase responsible for superoxide formation, such as p22^{phox}, gp91^{phox}, p47^{phox}, p40^{phox} and p67^{phox} (Figure 6H,I). Liver tissues were also tested to further validate the antioxidative roles. We found that D-PDMP and atorvastatin reduced hepatic oxidative stress, as evidenced by increased levels of T-AOC and GSH and decreased levels of MDA (Figure 3K–M). However, the hepatic levels of SOD and CAT were not significantly elevated (Figure 3N,O). Taking these findings together, D-PDMP was able to reduce oxidative stress impairment, but this function was not clearly observed in myriocin-treated mice.

Myriocin and D-PDMP attenuate vascular inflammation in part due to reduced phosphorylated ERK and nuclear factor-κB

We sought to understand the major signaling pathways that underlie myriocin- and D-PDMP-induced atheroprotection. Accumulating evidence has highlighted the critical roles played by MAP kinase (p38, ERK and JNK) and nuclear factor-κB (NF-κB) signaling pathways in inflammatory responses [20]. Compared with the vehicle group,

PORTLAND PRESS

Clinical Science (2020) **134** 439–458
https://doi.org/10.1042/CS20191028

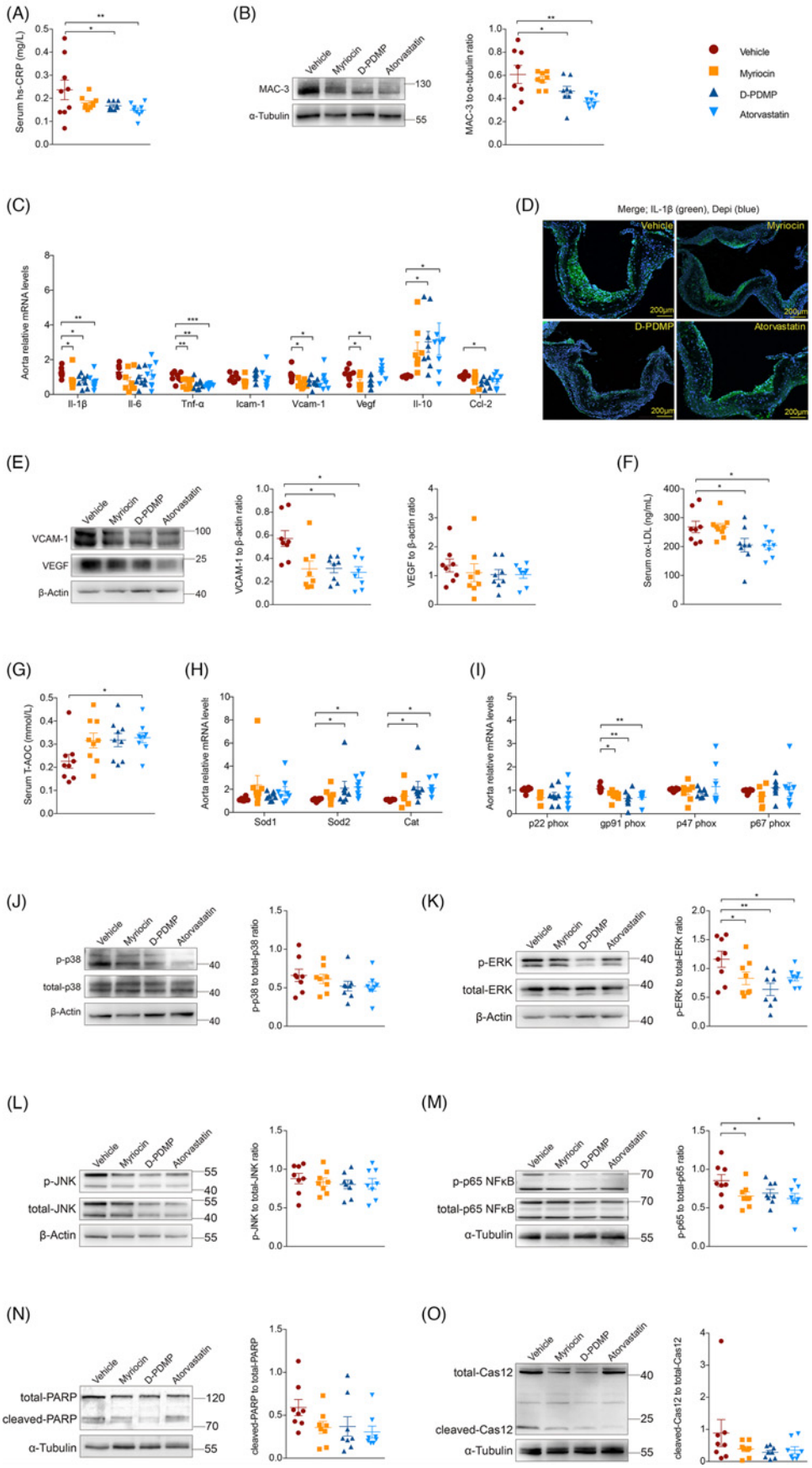

Figure 6. Myriocin and D-PDMP mediated anti-inflammatory functions by attenuating ERK and nuclear factor-κB activation, and oxidative stress impairment was markedly reduced in the D-PDMP-treatment group

(**A**) Concentration of the inflammatory marker, hs-CRP, in serum; n=9. (**B**) Aortic MAC-3 protein expression; n=8. (**C**) Relative expression levels of cytokine and chemokine mRNA in aortas; n=8. (**D**) Representative images of immunostaining for IL-1β in aortic-root lesions. (**E**) Aortic VCAM-1 and VEGF protein expression; n=8. (**F**) Oxidized-LDL levels in serum; n=8–9. (**G**) T-AOC in serum; n=9. (**H**) Relative expression levels of mRNAs involved in aortic SOD and CAT; n=8. (**I**) Relative expression levels of mRNAs involved in the subunits of NADPH oxidases in aortas; n=8. (**J**) Protein expression of phosphorylation of and p38 MAPK in aortas; n=8. (**K**) Protein expression of phosphorylation of ERK in aortas; n=8. (**L**) Protein expression of phosphorylation of and JNK in aortas; n=8. (**M**) Protein expression of phosphorylation of and p65 NF-κB in aortas; n=8. (**N**) Activation of PARP in aortas; n=8. (**O**) Activation of Caspase12 in aortas. Phosphorylated and total proteins were examined by Western blotting and α-Tubulin and β-Actin were used as protein loading controls; n=8. All data are expressed as means ± SEM. Statistical significance was determined by one-way ANOVA. $^{*}P<0.05$ was considered significant, $^{**}P<0.01$, $^{***}P<0.001$. Abbreviation: NF-κB, nuclear factor-κB.

myriocin, D-PDMP and atorvastatin treatment reduced the phosphorylation of ERK by 28.5, 45.1 and 27.6%, respectively (Figure 6J–L). Significantly decreased NF-κB activation was shown in aortas treated with myriocin and statin (Figure 6M). Ceramides have been identified as an inducer of apoptosis associated with lipotoxic cardiomyopathy [21]. The activation of apoptotic pathways was investigated but neither cleaved PARP or caspase-12 expression was significantly changed (Figure 6N,O).

Myriocin and D-PDMP were beneficial for maintaining whole-body glucose homeostasis

No significant differences in fasting blood-glucose levels were observed among the four groups (Figure 7A) or in the OGTT at the end of week 24 (Figure 7B,C). However, glucose levels in the mice were elevated along with the HFD feeding. Notably, the fasting insulin level and the IR index in myriocin-treated mice and D-PDMP-treated mice were lower compared with atorvastatin-treated mice (Figure 7D,E). The serum level of adiponectin, an anti-diabetic adipokine, was relatively elevated, indicating an improvement in systemic insulin sensitivity (Figure 7F). Additionally, taking into account the fact that the phosphorylation of AKT plays a key role in insulin signaling, immunoblots of phosphorylated and total AKT from the liver were performed. Compared with the vehicle-control group, p-AKT levels were elevated in the livers of animals treated with myriocin or D-PDMP (Figure 7G). Taking these findings together, and considering the association between statins and diabetes, these new sphingolipid inhibitors may probably be an adjunct to or a replacement for statin therapy.

Gonadal fat-pad mass in myriocin-treated apoE$^{-/-}$ mice was substantially decreased

We observed similar curves for body mass and comparable body masses among all treatment groups (Supplementary Figure S5A). Mice treated with myriocin ate 6.5% less food during the first month compared with the vehicle-treated animals (Supplementary Figure S5B). Nevertheless, there were no significantly different food efficiencies among the groups (Supplementary Figure S5C). A previous study reported that myriocin decreased the total fat mass in obese mice [22]. Herein, we evaluated the mass of white adipose tissue (WAT), including gonadal, perirenal and subcutaneous WAT (gWAT, pWAT and sWAT) and brown adipose tissue (BAT) in apoE$^{-/-}$ mice. We also performed histological analyses. The cross-sectional area of gWAT in myriocin-treated mice was noticeably smaller (Figure 7H). Myriocin decreased the mass of WAT after normalizing for body mass (Figure 7I,L,M). However, we observed a trend of increasing BAT mass in these mice (Figure 7N). F4/80 immunohistochemistry staining confirmed that fat pads in mice from the myriocin-treated group had far fewer infiltrated macrophages compared with those of vehicle-treated mice, indicating a reduction in adipose inflammation (Figure 7J,K).

Discussion

The present study is aimed to elucidate the therapeutic efficacy of sphingolipid inhibitors in improving atherosclerosis. Importantly, we identified the mechanisms which are intrinsically involved in vascular lipid-uptake and inflammatory responses (Figure 8). Treatment with myriocin and D-PDMP reduced aortic plaque sizes in atherogenic apoE$^{-/-}$ mice by approximately 35 and 25%, respectively, while atorvastatin reduced aortic plaque sizes by 30%. Interestingly, unlike atorvastatin, myriocin showed a mild ability to reduce serum LDL-C and VLDL-C, while D-PDMP rarely reduced cholesterol levels. Therefore, it is logical to hypothesize that the essential role of sphingolipid inhibitors is

Clinical Science (2020) **134** 439–458
https://doi.org/10.1042/CS20191028

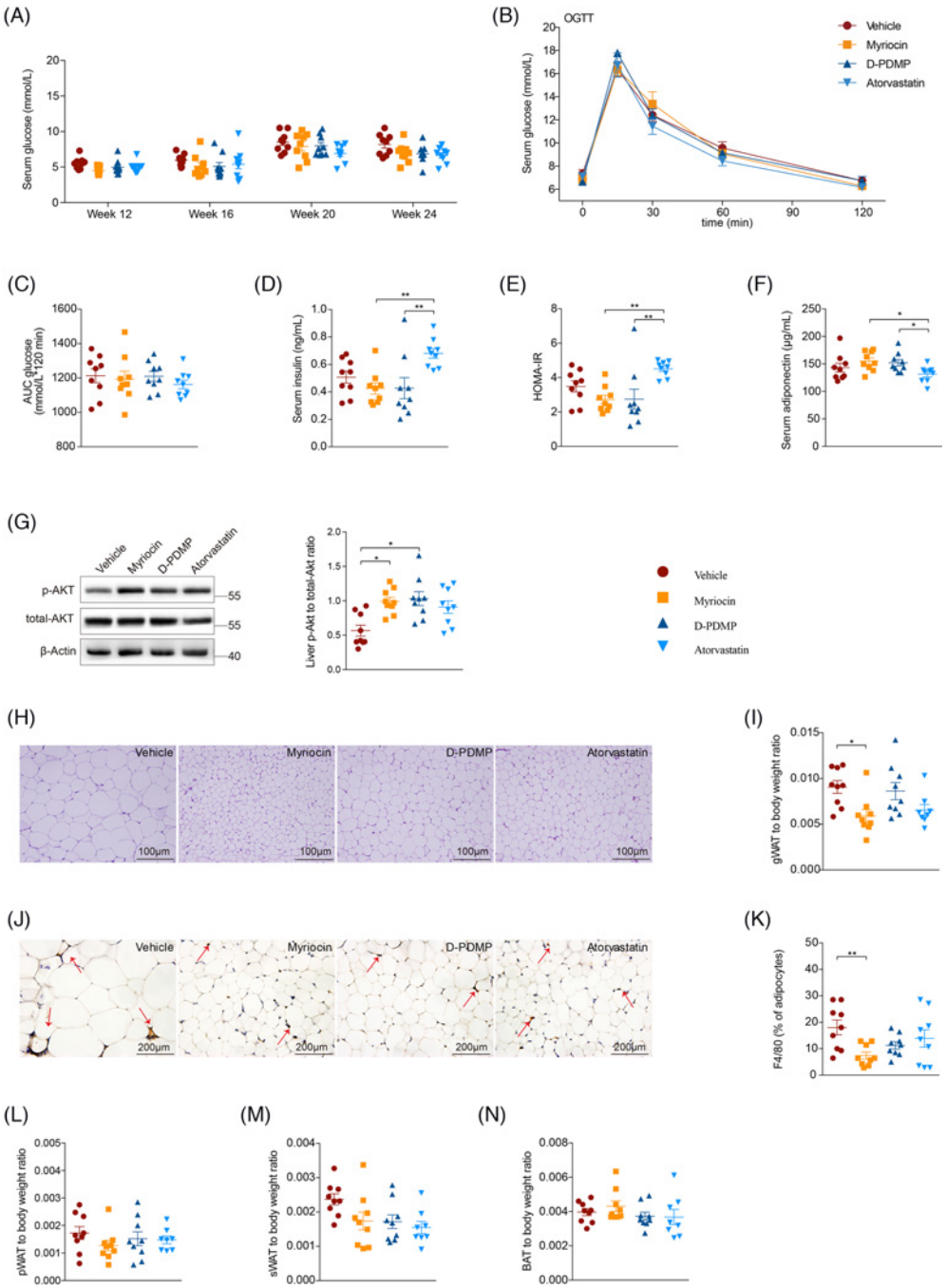

Figure 7. Myriocin and D-PDMP helped in maintaining whole-body glucose homeostasis in apoE$^{-/-}$ mice on an HFD; the masses of fat-pads in myriocin-treated mice were substantially reduced

(**A**) Fasting blood-glucose levels were measured every 4 weeks; n=9. (**B**) Circulating glucose levels were measured during an OGTT at week 24 (2.5 g/kg glucose per oral gavage); n=9. (**C**) AUC for serum glucose; n=9. (**D**) Fasting serum-insulin levels were quantified using ELISA; n=9. (**E**) HOMA-IR index was calculated; n=9. (**F**) Serum adiponectin levels were quantified using ELISA; n=9. (**G**) Representative immunoblots of phosphorylated and total Akt of liver samples from vehicle-, myriocin-, D-PDMP- and atorvastatin-treated mice. The bar graphs on the right represent relative protein quantification; n=9. (**H**) Representative images of H&E staining of gonadal fat-pads. (**I**) Gonadal fat-pad masses after normalizing to body mass; n=8–9. (**J**) Representative images of F4/80 staining of gonadal fat-pads. (**K**) Quantification of F4/80-positive cells (brown); n=9. (**L**) Perirenal adipose tissue masses after normalizing to body mass; n=8–9. (**M**) Subcutaneous adipose tissue masses after normalizing to body mass; n=8–9. (**N**) Brown adipose tissue masses after normalizing to body mass; n=8–9. All data are expressed as means ± SEM. Statistical significance was determined by one-way ANOVA. *P<0.05 was considered significant, **P<0.01.

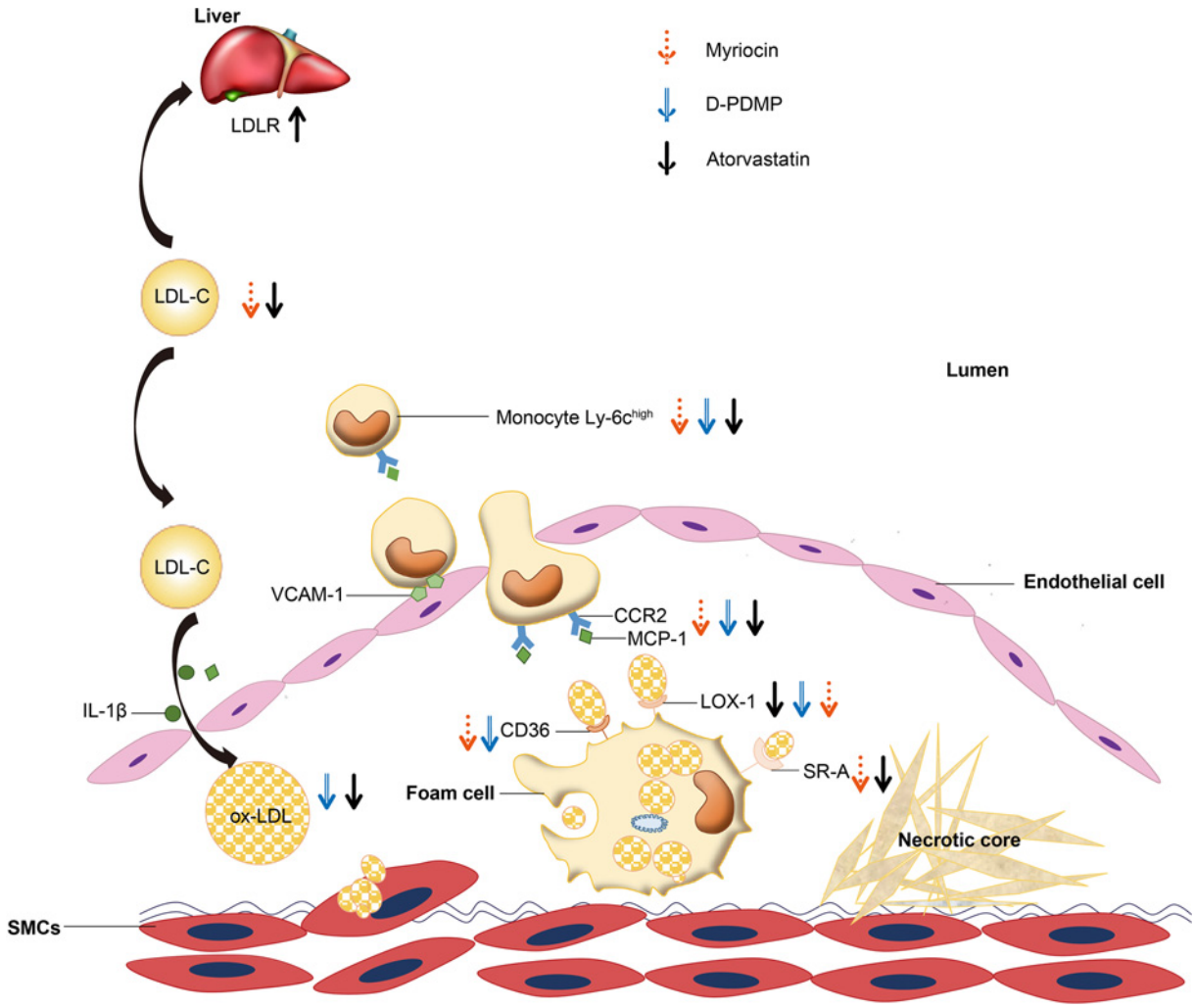

Figure 8. A proposed model for the roles of myriocin, D-PDMP and atorvastatin in atherosclerosis

Atorvastatin lowers circulating LDL-C by up-regulating hepatic LDLR. Myriocin lowers SM levels, resulting in a slight reduction in LDL-C. D-PDMP does not exhibit any cholesterol lowering ability but plays an antioxidant role in reducing ox-LDL. Myriocin and D-PDMP regulate the formation of foam cells by skewing monocytes away from the Ly-6c^{high} phenotype and suppressing the expression of scavenger receptors, such as CD36, LOX-1 and SR-A. In addition, the vascular inflammatory response was compromised by myriocin and D-PDMP.

not related to reducing serum cholesterols. To address this hypothesis, we investigated the major lipid metabolism pathways in the liver. Interestingly, Chatterjee et al. [10] has shown that D-PDMP decreased the level of serum TG and cholesterol via recruiting multiple genes. However, no significant alterations in TG metabolism or cholesterol metabolism, including cholesterol efflux, were seen with D-PDMP treatment in our study. The reasons for this are presently not clear. The nearly normal serum TG levels in all groups could probably explain why all treatments had no effects on TG metabolism. Besides, the medication time may partly explain the different effects on LDL-C levels, as according to their reported data, 24- or 16-weeks D-PDMP treatment approximately reduced serum LDL-C levels by 70% or 30% [10,23]. But above all, the data do suggest that D-PDMP could inhibit atherosclerosis, although serum cholesterols were not reduced below some certain threshold.

Smaller plaque sizes represent reduced lipid accumulation, which is associated with monocyte recruitment and foam-cell formation. We were intrigued to find out whether these sphingolipid inhibitors might be involved in skewing monocyte differentiation, since the Ly-6c^{high} phenotype has been reported to express higher levels of CD36 and possess a greater capacity to form foam cells [16]. We discovered for the first time that pharmacologically inhibiting sphingolipid synthesis plays a role in suppression monocytes differentiate toward Ly-6c^{high} phenotype. Indeed,

Clinical Science (2020) **134** 439–458
https://doi.org/10.1042/CS20191028

aortic CD36 expression was suppressed by myriocin and D-PDMP. CD36, LOX-1 and SR-A receptors are responsible for approximately 90% of ox-LDL uptake. Both inhibitors significantly inhibited the enhanced expression of LOX-1. SR-A expression was not markedly decreased by D-PDMP treatment. Also, impaired cholesterol efflux contributes to foam-cell formation. In our study, negligible improvements in lipid efflux were shown, since ABCG1 is considered to be crucial for cholesterol unloading. Thus, the present study identified the inhibition of lipid uptake as one of the mechanisms behind the athero-protective function of myriocin and D-PDMP.

Inflammation is intimately involved in foam-cell formation and plaque stability, contributing to all stages of atherosclerosis. The Ly-6c^{high} monocyte subset was termed as inflammatory classical cells that could release proinflammatory cytokines, such as IL-1, IL-6, TNF-α and MCP-1, which contribute to vascular dysfunction and lipid-laden foam cells accumulation [24]. The three compounds inhibited inflammatory monocyte diffentiation. Then, we observed that myriocin might attenuate inflammatory responses through the ERK and NF-κB pathways. D-PDMP might exert both anti-inflammatory and anti-oxidative functions via decreased ERK activation. Since increased lipid-raft levels are associated with inflammation, we measured the expression of Caveolin-1, a raft-specific marker [7,25]. A reduction in Caveolin-1 protein was found in D-PDMP-treated aortas (Figure 5L). Therefore, myriocin and D-PDMP were shown to be capable of improving atherosclerosis as a result of their anti-inflammatory properties.

Numerous data support the pronounced efficacy of 'sphingolipid reduction therapies' for improving IR in obese mice [26,27]. We observed a slight improvement in glucose metabolism in mice treated with myriocin and D-PDMP compared with statin-treated mice. It was previously reported that obese mice treated with myriocin displayed decreased adiposity, which was associated with increased energy expenditure [22]. We found similar adipose remodeling in myriocin-treated apoE$^{-/-}$ mice: their gWAT mass was substantially reduced and their BAT mass was relatively increased. To the best of our knowledge, iminosugar N-(5′-adamantane-1′-yl-methoxy)-pentyl-1-deoxynojirimycin (AMP-DNM) has been reported to improve adipose function [27]. In this study, reduced numbers of large adipocytes and a reduced inflammatory state were observed in D-PDMP-treated adipose tissue, but these findings were not statistically significant compared with the control group. A recent study reported that statins cause cell-autonomous impairment in insulin-stimulated adipocyte lipogenesis [28]. Here, the mass of atorvastatin-treated fat tissue displayed a similar downward trend, but the number of F4/80-positive cells did not noticeably decrease. The underlying regulatory mechanisms remain incompletely understood.

There were a number of limitations to the present study. We cannot rule out the possible contribution of apoE deficiency to whole-body metabolism. In addition, the possible side effects of the drugs, such as muscle pain due to statin therapy, were not adequately taken into account. Statin treatment in combination with myriocin or D-PDMP will be further analyzed in future studies.

Overall, myriocin and D-PDMP treatment were sufficiently effective at reducing and stabilizing atherosclerotic plaques. Unlike atorvastatin, their athero-protective roles were not primarily dependent on the reduction in serum cholesterols. This mechanistic study indicated that sphingolipid inhibitors reduce the formation of foam cells as a result of decreased lipid uptake, rather than enhanced reverse cholesterol transport. Furthermore, their anti-inflammatory roles were also proved. Myriocin and D-PDMP appear to be an effective replacement for or adjunct to statin therapy, which would possibly provide a two-pronged approach for treating atherosclerosis. Moreover, these sphingolipid inhibitors performed better at maintaining a normal glucose level compared with atorvastatin and therefore we postulate that, in clinical practice, they may be promising avenues to explore for concurrently combating atherosclerosis and diabetes.

Clinical perspectives

- Many human studies have identified ceramides as strong risk markers for major adverse cardiac events, and the fundamental pathological process underlying these vascular diseases is atherosclerosis. Studies in rodents indicated that pharmacologically inhibiting ceramide biosynthesis ameliorates atherosclerotic plaque progression. However, whether inhibiting glycosphingolipid synthesis *per se* also exerts an anti-atherogenic effect remains uncertain. The present study extensively interrogated the effects of two novel potential therapeutic moieties in the treatment of atherosclerosis and tried to elucidate the underlying mechanisms.

- We found that treatment with sphingolipid inhibitors (myriocin or D-PDMP) led to smaller and less vulnerable atherosclerotic lesions and was almost as effective as atorvastatin. Unlike atorvastatin,

the athero-protective roles of myriocin and D-PDMP are not primarily dependent on the reduction of LDL-C. These sphingolipid inhibitors performed better at maintaining a normal glucose level compared with atorvastatin. Noticeably, we discovered for the first time that pharmacologically inhibiting sphingolipid synthesis plays a role in suppressing monocytes that differentiate toward a Ly-6c^{high} phenotype. Moreover, the modulation of sphingolipid synthesis can effectively alleviate atherosclerosis progression by preventing lipid uptake and reducing inflammatory responses in the arterial walls.

- Our results provide evidence for the efficacy of ceramide glucosyltransferase inhibitors. Specifically, we focused on how the mechanisms of sphingolipid inhibitors combat atherosclerosis by down-regulating lipid uptake and inflammation. These inhibitors offer prospects in clinical applications for vascular diseases, such as treatments in conjunction with existing lipid-lowering therapies, or for treating patients who are resistant or intolerant to statins, patients with normal LDL-C but who are still at a high risk of adverse events and patients with diabetes.

Competing Interests

The authors declare that there are no competing interests associated with the manuscript.

Funding

This work was supported by the Fundamental Research Funds for the Central Universities, Peking University Medicine Seed Fund for Interdisciplinary Research [grant number BMU2017MC005]; and the Funds for National Science and Technology Major Project [grant number 2012ZX09303-005-003].

Author Contribution

Conception and design: Zemou Yu, Qing Peng, Yu Bai. Development of methodology: Zemou Yu, Yu Bai, Songyue Li, Hongjun Hao. Acquisition of data: Zemou Yu, Zhiyuan Shen, Songyue Li, Jianwen Deng, Weiwei Yu, Ding Nan. Analysis and interpretation of data (e.g. statistical analysis, biostatistics, computational analysis): Zemou Yu, Songyue Li, Lingbing Meng, Yining Huang, Yu Bai. Writing, review, and/or revision of the manuscript: Zemou Yu, Yining Huang, Lingbing Meng. Administrative, technical, or material support: Qing Peng, Yu Bai, Hongjun Hao, Yining Huang. Study supervision: Qing Peng, Yu Bai, Yining Huang.

Abbreviations

ABCG1, ATP-binding cassette transporter G1; ACAT1, acyl-coenzyme A cholesterol acyltransferase 1; ALT, alanine aminotransferase; ApoE$^{-/-}$, apolipoprotein E-deficient; AST, aspartate aminotransferase; BAT, brown adipose tissue; CAT, catalase; Ccl2, chemokine (C-C motif) ligand 2; CCR2, chemoattractant cytokine receptor 2; CD36, cluster of differentiation 36; CVD, cardio-cerebral vascular disease; D-PDMP, D-threo-1-phenyl-2-decanoylamino-3-morpholino-1-propanol; ECG, electrocardiogram; ERK, extracellular signal-regulated protein kinas; GSH, glutathione; gWAT, gonadal white adipose tissue; HDL-C, high-density lipoprotein cholesterol; HFD, high-fat diet; HOMA, homeostatic model assessment; hs-CRP, high-sensitivity C-reactive protein; H&E, Hematoxylin and Eosin; Icam-1, intervascular cell adhesion molecule-1; IPP, Image-Pro Plus; IR, insulin resistance; JNK, c-Jun-N-terminal protein kinase; LDL-C, low-density lipoprotein cholesterol; LOX-1, lectin-like oxidized LDL receptor-1; MAC-3, macrophage antigen-3; MCP-1, monocyte chemotactic protein 1; MDA, malondialdehyde; NF-κB, nuclear factor-κB; OGTT, oral glucose tolerance test; ox-LDL, oxidized LDL; PARP, poly ADP-ribose polymerase; PBS, phosphate-buffered saline; PWV, pulse wave velocity; SM, sphingomyelin; SMC, smooth muscle cell; SOD, superoxide dismutase; SPT, serine palmitoyltransferase; SR-A, scavenger receptor-A; sWAT, subcutaneous white adipose tissue; TC, total cholesterol; TG, triglyceride; TNF-α, tumor necrosis factor α; T-AOC, total antioxidant capacity; Vcam-1, vascular cell adhesion molecule-1; WAT, white adipose tissue; α-SMA, α-smooth musle actin.

References

1 Wilson, P.W.F., Polonsky, T.S., Miedema, M.D., Khera, A., Kosinski, A.S. and Kuvin, J.T. (2019) Systematic review for the 2018 AHA/ACC/AACVPR/AAPA/ABC/ACPM/ADA/AGS/APhA/ASPC/NLA/PCNA guideline on the management of blood cholesterol: a report of the American College of Cardiology/American Heart Association Task Force on Clinical Practice Guidelines. *Circulation* **139**, e1144–e1161, https://doi.org/10.1161/CIR.0000000000000626

2 Fernandez-Ruiz, I. (2019) Statin efficacy in primary CVD prevention might diminish with patient age. *Nat. Rev. Cardiol.* **16**, 200–200, https://doi.org/10.1038/s41569-019-0171-8

Clinical Science (2020) **134** 439–458
https://doi.org/10.1042/CS20191028

3 Ahmadizar, F., Ochoa-Rosales, C., Glisic, M., Franco, O.H., Muka, T. and Stricker, B.H. (2019) Associations of statin use with glycaemic traits and incident type 2 diabetes. *Br. J. Clin. Pharmacol.* **85**, 993–1002, https://doi.org/10.1111/bcp.13898
4 Holland, W.L. and Summers, S.A. (2018) Strong heart, low ceramides. *Diabetes* **67**, 1457–1460, https://doi.org/10.2337/dbi18-0018
5 Summers, S.A. (2018) Could ceramides become the new cholesterol? *Cell Metab.* **27**, 276–280, https://doi.org/10.1016/j.cmet.2017.12.003
6 Park, T.S., Panek, R.L., Mueller, S.B., Hanselman, J.C., Rosebury, W.S., Robertson, A.W. et al. (2004) Inhibition of sphingomyelin synthesis reduces atherogenesis in apolipoprotein E-knockout mice. *Circulation* **110**, 3465–3471, https://doi.org/10.1161/01.CIR.0000148370.60535.22
7 Chakraborty, M., Lou, C., Huan, C., Kuo, M.S., Park, T.S., Cao, G. et al. (2013) Myeloid cell-specific serine palmitoyltransferase subunit 2 haploinsufficiency reduces murine atherosclerosis. *J. Clin. Invest.* **123**, 1784–1797, https://doi.org/10.1172/JCI60415
8 Hannun, Y.A. and Obeid, L.M. (2018) Sphingolipids and their metabolism in physiology and disease. *Nat. Rev. Mol. Cell Biol.* **19**, 175–191, https://doi.org/10.1038/nrm.2017.107
9 Glaros, E.N., Kim, W.S., Rye, K.A., Shayman, J.A. and Garner, B. (2008) Reduction of plasma glycosphingolipid levels has no impact on atherosclerosis in apolipoprotein E-null mice. *J. Lipid Res.* **49**, 1677–1681, https://doi.org/10.1194/jlr.E800005-JLR200
10 Chatterjee, S., Bedja, D., Mishra, S., Amuzie, C., Avolio, A., Kass, D.A. et al. (2014) Inhibition of glycosphingolipid synthesis ameliorates atherosclerosis and arterial stiffness in apolipoprotein E-/- mice and rabbits fed a high-fat and -cholesterol diet. *Circulation* **129**, 2403–2413, https://doi.org/10.1161/CIRCULATIONAHA.113.007559
11 Bietrix, F., Lombardo, E., van Roomen, C.P., Ottenhoff, R., Vos, M., Rensen, P.C. et al. (2010) Inhibition of glycosphingolipid synthesis induces a profound reduction of plasma cholesterol and inhibits atherosclerosis development in APOE*3 Leiden and low-density lipoprotein receptor-/- mice. *Arterioscler. Thromb. Vasc. Biol.* **30**, 931–937, https://doi.org/10.1161/ATVBAHA.109.201673
12 Drouin-Chartier, J.P., Tremblay, A.J., Bergeron, J., Lamarche, B. and Couture, P. (2017) The low-density lipoprotein receptor genotype is a significant determinant of the rebound in low-density lipoprotein cholesterol concentration after lipoprotein apheresis among patients with homozygous familial hypercholesterolemia. *Circulation* **136**, 880–882, https://doi.org/10.1161/CIRCULATIONAHA.117.029435
13 Yu, Z., Peng, Q. and Huang, Y. (2019) Potential therapeutic targets for atherosclerosis in sphingolipid metabolism. *Clin. Sci.* **133**, 763–776, https://doi.org/10.1042/CS20180911
14 Bijl, N., Sokolović, M., Vrins, C., Langeveld, M., Moerland, P.D., Ottenhoff, R. et al. (2009) Modulation of glycosphingolipid metabolism significantly improves hepatic insulin sensitivity and reverses hepatic steatosis in mice. *Hepatology* **50**, 1431–1441, https://doi.org/10.1002/hep.23175
15 Chaurasia, B., Tippetts, T.S., Mayoral Monibas, R., Liu, J., Li, Y., Wang, L. et al. (2019) Targeting a ceramide double bond improves insulin resistance and hepatic steatosis. *Science* **365**, 386–392, https://doi.org/10.1126/science.aav3722
16 Raghavan, S., Singh, N.K., Gali, S., Mani, A.M. and Rao, G.N. (2018) Protein kinase C via activating transcription factor 2-mediated CD36 expression and foam cell formation of Ly6C(hi) cells contributes to atherosclerosis. *Circulation* **138**, 2395–2412, https://doi.org/10.1161/CIRCULATIONAHA.118.034083
17 Fan, J., Liu, L., Liu, Q., Cui, Y., Yao, B., Zhang, M. et al. (2019) CKIP-1 limits foam cell formation and inhibits atherosclerosis by promoting degradation of Oct-1 by REGgamma. *Nat. Commun.* **10**, 425, https://doi.org/10.1038/s41467-018-07895-3
18 Conte, M., Franceschi, C., Sandri, M. and Salvioli, S. (2016) Perilipin 2 and age-related metabolic diseases: a new perspective. *Trends Endocrinol. Metab.* **27**, 893–903, https://doi.org/10.1016/j.tem.2016.09.001
19 Dekker, M.J., Baker, C., Naples, M., Samsoondar, J., Zhang, R., Qiu, W. et al. (2013) Inhibition of sphingolipid synthesis improves dyslipidemia in the diet-induced hamster model of insulin resistance: evidence for the role of sphingosine and sphinganine in hepatic VLDL-apoB100 overproduction. *Atherosclerosis* **228**, 98–109, https://doi.org/10.1016/j.atherosclerosis.2013.01.041
20 Bandaru, S., Ala, C., Salimi, R., Akula, M.K., Ekstrand, M., Devarakonda, S. et al. (2019) Targeting Filamin A reduces macrophage activity and atherosclerosis. *Circulation* **140**, 67–79, https://doi.org/10.1161/CIRCULATIONAHA.119.039697
21 Walls, S.M., Cammarato, A., Chatfield, D.A., Ocorr, K., Harris, G.L. and Bodmer, R. (2018) Ceramide-protein interactions modulate ceramide-associated lipotoxic cardiomyopathy. *Cell Rep.* **22**, 2702–2715, https://doi.org/10.1016/j.celrep.2018.02.034
22 Chaurasia, B., Kaddai, V.A., Lancaster, G.I., Henstridge, D.C., Sriram, S., Galam, D.L. et al. (2016) Adipocyte ceramides regulate subcutaneous adipose browning, inflammation, and metabolism. *Cell Metab.* **24**, 820–834, https://doi.org/10.1016/j.cmet.2016.10.002
23 Mishra, S., Bedja, D., Amuzie, C., Foss, C.A., Pomper, M.G., Bhattacharya, R. et al. (2015) Improved intervention of atherosclerosis and cardiac hypertrophy through biodegradable polymer-encapsulated delivery of glycosphingolipid inhibitor. *Biomaterials* **64**, 125–135, https://doi.org/10.1016/j.biomaterials.2015.06.001
24 Fang, P., Li, X., Shan, H., Saredy, J.J., Cueto, R., Xia, J. et al. (2019) Ly6C(+) inflammatory monocyte differentiation partially mediates hyperhomocysteinemia-induced vascular dysfunction in type 2 Diabetic db/db mice. *Arterioscler. Thromb. Vasc. Biol.* **39**, 2097–2119, https://doi.org/10.1161/ATVBAHA.119.313138
25 Ramlrez, C.M., Zhang, X., Bandyopadhyay, C., Rotllan, N., Sugiyama, M.G., Aryal, B. et al. (2019) Caveolin-1 regulates atherogenesis by attenuating LDL transcytosis and vascular inflammation independent of endothelial nitric oxide synthase activation. *Circulation* **140**, 225–239, https://doi.org/10.1161/CIRCULATIONAHA.118.038571
26 Hammerschmidt, P., Ostkotte, D., Nolte, H., Gerl, M.J., Jais, A., Brunner, H.L. et al. (2019) CerS6-derived sphingolipids interact with Mff and promote mitochondrial fragmentation in obesity. *Cell* **177**, 1536–1552.e1523, https://doi.org/10.1016/j.cell.2019.05.008
27 van Eijk, M., Aten, J., Bijl, N., Ottenhoff, R., van Roomen, C.P., Dubbelhuis, P.F. et al. (2009) Reducing glycosphingolipid content in adipose tissue of obese mice restores insulin sensitivity, adipogenesis and reduces inflammation. *PLoS ONE* **4**, e4723, https://doi.org/10.1371/journal.pone.0004723
28 Henriksbo, B.D., Tamrakar, A.K., Xu, J., Duggan, B.M., Cavallari, J.F., Phulka, J. et al. (2019) Statins promote interleukin-1beta-dependent adipocyte insulin resistance through lower prenylation, not cholesterol. *Diabetes* **68**, 1441–1448, https://doi.org/10.2337/db18-0999